INL/RPT-23-75024-Rev000

# Develop and Connect TRISO Failure Analysis and Uncertainty Quantification to Fission Product Release Calculation Capability

September 2023

*Technical Report*

Antonio M. Recuero[1], Gyanender Singh[1], Wen Jiang[1], and Ryan Sweet[1]

[1]Idaho National Laboratory

Idaho National Laboratory

*INL is a U.S. Department of Energy National Laboratory operated by Battelle Energy Alliance, LLC*

# Develop and Connect TRISO Failure Analysis and Uncertainty Quantification to Fission Product Release Calculation Capability

**Technical Report**

Antonio M. Recuero[1], Gyanender Singh[1], Wen Jiang[1], and Ryan Sweet[1]

[1]Idaho National Laboratory

**September 2023**

**Idaho National Laboratory**
**Computational Mechanics and Materials Department**
**Idaho Falls, Idaho 83415**

**http://www.inl.gov**

**Prepared for the**
**U.S. Department of Energy**
**Office of Nuclear Energy**
**Under U.S. Department of Energy-Idaho Operations Office**
**Contract DE-AC07-05ID14517**

*Page intentionally left blank*

# ABSTRACT

The U.S. Department of Energy's Nuclear Energy Advanced Modeling and Simulation (NEAMS) program aims to develop predictive capabilities by applying computational methods to the analysis and design of advanced reactor and fuel cycle systems. This program has been providing engineering-scale support for the development of BISON, a high-fidelity and high-resolution fuel performance tool.

Stress-based failure probability has been developed and analyzed to assess the integrity of tri-structural isotropic (TRISO) fuel particles during fuel life cycles. While simple, stress-based approaches to failure probability leveraging the Weibull statistical distribution entails a number of drawbacks when stress concentration occurs near crack tips, including finite element mesh size dependency. In this report, we use an interaction integral approach to the computation of stress intensity factors in functionally graded materials (FGM) for axisymmetric models. The inner pyrolytic carbon (IPyC) cracking induced silicon carbide (SiC) failure is one of the dominated failure modes in TRISO failure analysis. In this study, we consider a crack in the IPyC layer perpendicular to the SiC layer. The interface between these two TRISO layers is considered to be porous, which we simulate considering a transition of mechanical properties over the porous length. These aspects are considered in the computation of stress intensity factor (SIF) from a fracture mechanics approach and compared with the known stress-based failure probability approach.

## Acknowledgment

This report was authored by a contractor of the U.S. Government under contract no. DE-AC07-05ID14517. Accordingly, the U.S. Government retains a non-exclusive, royalty-free license to publish or reproduce the published form of this contribution, or allow others to do so, for U.S. Government purposes.

This research made use of the resources of the High Performance Computing Center at Idaho National Laboratory (INL), which is supported by the Office of Nuclear Energy of the U.S. Department of Energy and the Nuclear Science User Facilities under contract no. DE-AC07-05ID14517.

## Orcid

Antonio Recuero 0000-0002-2611-1812
Gyanender Singh 0000-0003-1828-4438
Wen Jiang 0000-0001-6978-9159
Ryan Sweet 0000-0002-7919-4623

# Contents

# List of Figures

# List of Tables

# Listings

## Acronyms

| | |
|---|---|
| **SIF** | stress intensity factor |
| **DOE** | U.S. Department of Energy |
| **FGM** | functionally graded materials |
| **INL** | Idaho National Laboratory |
| **IPyC** | inner pyrolytic carbon |
| **MOOSE** | Multiphysics Object-Oriented Simulation Environment |
| **NEAMS** | Nuclear Energy Advanced Modeling and Simulation |
| **SiC** | silicon carbide |
| **SIF** | stress intensity factor |
| **TRISO** | tri-structural isotropic |

# 1. INTRODUCTION

A stress-based approach for estimating the failure probability was developed and demonstrated to assess the integrity of TRI-structural ISO-tropic (TRISO) particles during fuel life cycles in recent work (see Jiang et al. (2022)). While simple, a stress-based approach to estimate failure probability, leveraging the Weibull statistical distribution, entails a number of drawbacks, including finite element mesh size dependency. In this report, we present a fracture mechanics-based approach to compute the stress intensity factors (SIFs) in functionally graded materials (FGM) for axisymmetric models. We consider a crack in a TRISO inner pyrolytic carbon (IPyC) layer perpendicular to the silicon carbide (SiC) layer. The interface between both TRISO layers is considered to be porous, which we model via a transition of mechanical properties over the porous length. These aspects are considered in the computation of an SIF from a fracture mechanics approach and compared with the known stress-based failure probability approach. We also perform a sensitivity study to better understand the influence of material porosity, the thickness of the TRISO particle layers, and the relative stiffness of the IPyC/SiC layers.

An idea introduced in this report is the consideration of material grading on the IPyC/SiC interface for the structural solution. That modeling aspect, which is based on experimental observation, regularizes the fracture mechanics problem, which then yields non-trivial fracture metrics. Such fracture mechanics-based methodology for the assessment of TRISO particle structural integrity is presented herein as an improved strategy for predicting the failure probability of this type of nuclear fuel.

# 2. DOMAIN INTEGRAL APPROACH FOR COMPUTING SIF

## 2.1 Interaction Integral Approach

The Multiphysics Object-Oriented Simulation Environment (MOOSE) framework features the ability to compute path integrals using domain integration. This feature is used to obtain J-integral values and SIFs via a domain interaction integral. These capabilities have been verified for homogeneous materials and Cartesian models. For the fracture analysis of TRISO particles, two additional aspects for the prediction of SIF using the interaction integral were identified. First, the analysis of a radial crack in a spherical particle can be studied using axisymmetric equations in two dimensions. Second, the porosity of TRISO layers can be mechanically modeled via a functional description of material parameters, such as FGM. These two developments have been carried out and verified in this work.

We expanded on the existing solid mechanics capabilities in MOOSE to generally determine the SIF of materials whose material properties vary through space according to some analytically-defined functions (i.e., FGM). We use here the "non-equilibrium" formulation to include space-dependency of elastic material properties. Particularly, we allow the isotropic elasticity modulus to vary according to an arbitrary analytical function. The domain integral-based approach we use to include the additional physics due to functional grading is introduced in Kim and Paulino (2004). This "non-equilibrium" formulation assumes the original auxiliary fields from homogeneous materials and defines the auxiliary stress field as $\sigma_{ij}^{\text{aux}} = C_{ijkl}(X)\epsilon_{kl}^{\text{aux}}$. This expression does not satisfy the equilibrium equation because it differs from $\sigma_{ij}^{\text{aux}} = C_{ijkl(\text{tip})}\epsilon_{kl}^{\text{aux}}$. The derivatives of the auxiliary stress field involve spatial derivatives of the elasticity tensor (i.e., $C_{ijkl,m}(X)$, in which $m$ denotes a global direction). By omitting the kinetic and thermal strain terms, the local form of the interaction integral may be written as follows:

$$M_1^{\text{local}} = \underbrace{\int_V \left(\sigma_{ij}u_{i,1}^{\text{aux}} + \sigma_{ij}^{\text{aux}}u_{i,1} - \sigma_{ik}\epsilon_{ik}^{\text{aux}}\delta_{1j}\right)\frac{\partial q}{\partial X_j}\mathrm{d}V}_{\text{Existing homogeneous terms}} + \underbrace{\int_V \left(C_{ijkl,j}(X)\epsilon_{kl}^{\text{aux}} - C_{ijkl,1}\epsilon_{kl}\epsilon_{ij}^{\text{aux}}\right)q\mathrm{d}V}_{\text{Non-equilibrium formulation}}, \tag{2.1}$$

where subscript 1 refers to the local direction of crack propagation and $q$ is a scalar that takes value from zero to one depending on whether the integral is evaluated within the domain. Assum-

ing mode I only deformation, one can obtain the stress intensity factor as $K_I = M_1^{\text{local}} E'_{\text{tip}}/2.0$. Note that $E'_{\text{tip}}$ refers to the material properties at the crack tip.

### 2.1.1 Verification

We verify the implementation of FGM in the interaction integral for the computation of SIF against two independent sets of results obtained by finite element methods. We use numerical results for a cracked plate under tension loading (see Figure 7 of Kim and Paulino (2003)). The SIFs used to verify the implementation of MOOSE are obtained from Kim and Paulino (2003) and Rao and Rahman (2003). A plane strain, two-dimensional model capturing the setup in Kim and Paulino (2003), but leveraging symmetry along the $X_2$ (Y) axis, was built in MOOSE. The crack is assumed to lie on the Y symmetry plane in our case. The material is assumed to transition from an elasticity modulus of 3 MPa to 1 MPa. $\bar{\epsilon}$, which denotes the axial strain imposed at one end of the cracked plate, is chosen to be 0.001. A boundary condition at the top surface is defined by such normal traction of $\sigma_{\text{traction}} = \bar{\epsilon}\bar{E}(X_1)$. We adopt here the following analytical form of the spatial distribution the material's Young's moduli.

$$E(X) = \frac{E_1 + E_2}{2} + \frac{E_1 - E_2}{2} \tanh\left(\beta\left[X_1 + 0.1\right]\right) \tag{2.2}$$

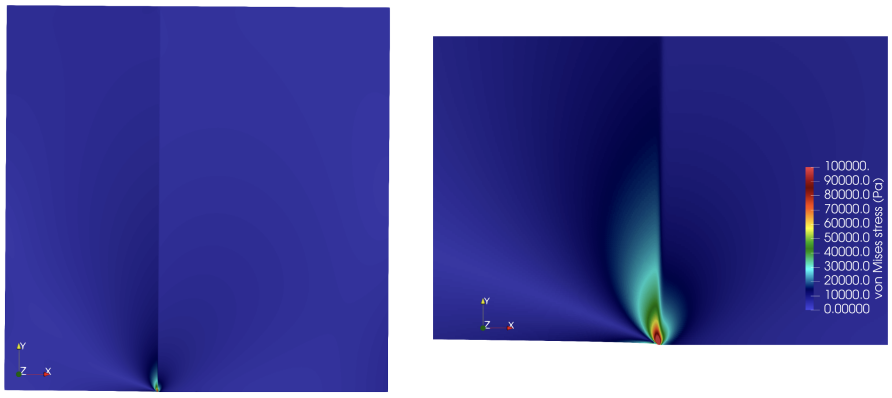


Figure 2.1. von Mises stress distribution in FGM with a narrow transition region in a cracked plate where the crack's mouth points to the left.

We vary the parameter $\beta$ in Equation 2.2. A value of $\beta = 0$ denotes a homogeneous material, whereas a value of $\beta = \infty$ describes a sharp interface with an infinite gradient (i.e., a theoretical bimaterial interface).

Figure 2.2 shows a normalized SIF for Mode I computed with MOOSE (using various levels of mesh refinement) and the numerical results from the references (Kim and Paulino, 2003; Rao and Rahman, 2003). A few aspects are noteworthy. (1) The results between Rao and Rahman

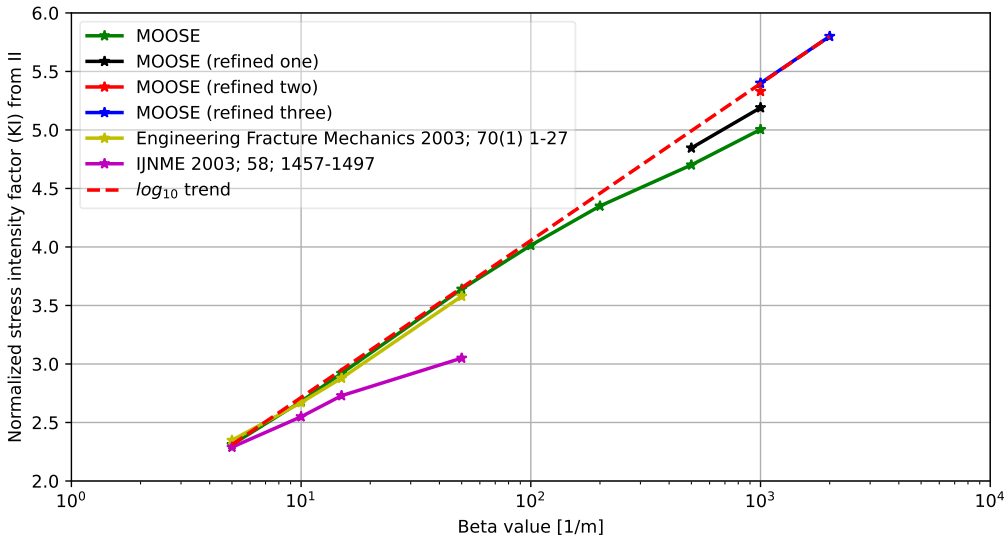


Figure 2.2. Verification of the implementation against published literature. Additional numerical results from MOOSE are provided to illustrate the effect of narrowing the area of transition of material properties. As the functionally-graded material tends to become a bimaterial, sharp interface, the SIF continues to grow.

(2003) and MOOSE agree very well for the values reported in the published article, where agreement with Kim and Paulino (2003) is of a lesser quality and a divergence is observed as the $\beta$ value becomes larger (i.e. transition region becomes narrower). (2) A sufficiently refined mesh is required to capture sharp material transitions. For example, for a value $\beta = 1000$, a few levels of mesh refinement are required. Refinement leads to larger SIFs for this setup, which means mesh convergence is a must to obtain conservative estimates of fracture[a]. The labels "refined one," "refined two," and "refined three" refer to additional levels of uniform refinement for one, two, and three additional levels, respectively. (3) SIFs continue to grow as the transition region over the "interface" becomes sharper. This relation is such that $K_I \propto \log_{10}(\beta) \propto \log_{10}(1/\Delta X_1)$. (4) Failure to consider "non-equilibrium" terms in the interaction integral may result in a severe underestimation of the risk of failure of graded materials with a sharp interface length (see Table 2.1). Note that the dependency of the SIFs with the size of the transition region obtained from the numerical results using the interaction integral is consistent with an analytical approach that uses dislocations of a crack perpendicular to a bimaterial interface, but at a distance $b$. In other words, as the distance of the crack to the bimaterial interface is linearly reduced, the resulting SIF increases (decreases) with $\propto \log_{10}(b)$ (see Figs. 2 and 3 in Wang and Ståhle (1998)) if the crack would extend into softer (stiffer) material.

To demonstrate the influence of the location of the crack, we swap the materials such that the

[a]Note that this mesh dependency is due to the need to accurately model the spatial evolution of material parameters (i.e., finer meshes are generally required to model sharper changes in material properties).

Table 2.1. Convergence of normalized SIF computed from the interaction integral. Dismissing terms that capture spatial variation of material properties may lead to severe underprediction of fracture risk.

| $\beta$ | Kim and Paulino (2003) | Rao and Rahman (2003) | Present Work | Uniform Interaction Integral |
|---|---|---|---|---|
| 5 | 2.289 | 2.348 | 2.310 | 2.232 |
| 10 | 2.549 | 2.670 | 2.681 | 2.518 |
| 15 | 2.729 | 2.879 | 2.923 | 2.600 |
| 50 | 3.050 | 3.579 | 3.639 | 2.842 |
| 500 | N.A. | N.A. | 4.787 | 2.975 |

crack exists in the softer subdomain. Repeating the numerical procedure that generated Figure 2.2, we obtain the following results shown in Figure 2.3. Note that, in this case, as the $\beta$ value increases (thus reducing the transition zone), the corresponding SIF value follows a descending trend. Also consistent with Wang and Ståhle (1998), Figure 2.3 shows that when approaching the theoretical limit, a crack located in this way will not propagate. Abrupt interfaces, however, may not always occur; the assumption of transition over a small region may be useful for layered materials as well, as discussed in the next section.

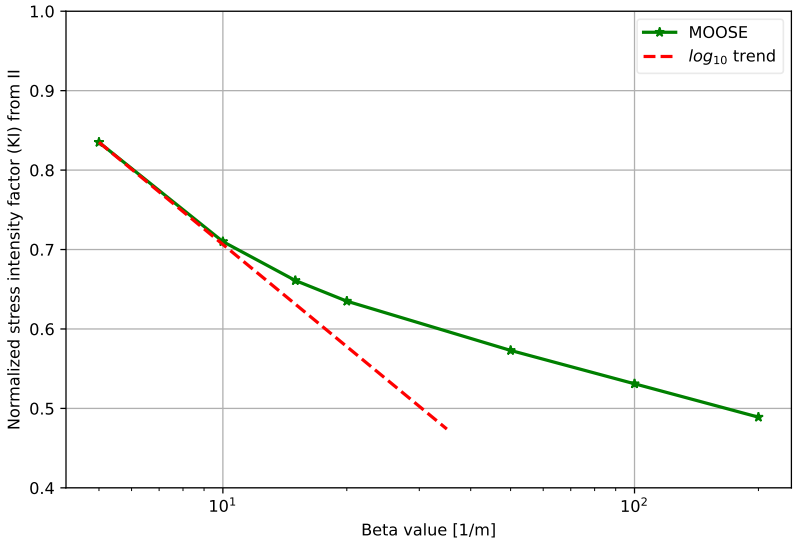


Figure 2.3. Sensitivity of crack SIF in softer material, extending into stiffer materials, with a transition region size (no refinement study is performed for this set of numerical results).

## 2.2 Development and Verification in Axisymmetric Coordinate System

The implementation of the interaction integral in MOOSE assumed Cartesian coordinates for two- and three-dimensional model setups. As part of the effort to develop a linear fracture mechanics approach to analyze failure in TRISO particles, we developed an axisymmetric ("RZ") form of the interaction integral terms. The axisymmetric form of the equations allow to study many thermomechanical problems with irradiation effects in two dimensions, without resorting to computationally costly three-dimensional finite element domains. Comparable to the first term of Equation 2.1, the interaction integral in the axisymmetric coordinate system can be described as follows:

$$\begin{aligned} M^{\text{local}}_{RZ,1} =& \frac{1}{R}\int_V \left[\sigma_{ij}u^{(aux)}_{j,1} + \sigma^{(aux)}_{ij}u_{j,1} - \sigma_{jk}\epsilon^{(aux)}_{jk}\delta_{1i}\right] q_{,i} \\ &+ \left[\left(\frac{u_1}{r}\sigma^{(aux)}_{\theta\theta}\right) + \frac{u^{(aux)}_1}{r}\sigma_{\theta\theta} - \sigma_{jk}\epsilon^{(aux)}_{jk}\right]\frac{q}{r} \\ &+ \frac{1}{r}\left[\sigma^{(aux)}_{1j}u_{j,1} - \sigma^{(aux)}_{\theta\theta}u_{1,1} + \sigma_{\theta\theta}\left(u^{(aux)}_{1,1} - \frac{u^{(aux)}_1}{r}\right)\right] qr\,\mathrm{d}V, \end{aligned} \tag{2.3}$$

where $R$ is the radial location of the crack, $r$ is a relative location with respect to the crack tip, $u^{(aux)}$ is the auxiliary displacement field, and 1 refers to the local direction of crack advancement, which in the case of a radial crack, would coincide with the radial direction. As the radius of the problem becomes larger, the axisymmetric result converges to the Cartesian numerical result (see Nahta and Moran (1993) for details). Note that this form of the interaction integral can be integrated with other features such as its application to functionally graded materials. FGM terms of Equation 2.1 apply also to Equation 2.3 within the axisymmetric form of the interaction integral.

The recently implemented axisymmetric interaction integral was verified against the results presented in the literature (see Van-Xuan and Samuel (2012); Shariati et al. (2017)). The problem is defined as follows: A solid cylinder with an internal radial crack with a crack radius to a cylinder radius ratio of 0.2 and a crack radius to a cylinder height ratio of 0.1, where a tensile, axial load of 1 MPa is applied. Results are given in Table 2.2.

Table 2.2. Convergence of SIF computed from the interaction integral for a solid cylinder with a circumferential crack with a sufficiently refined mesh. To analyze the fracture of TRISO particles in 2D-RZ problems, the new form of the interaction integral presented in Equation 2.3 is used.

| Van-Xuan and Samuel (2012) (analytical) | MOOSE (axisymm.) |
|---|---|
| 1.596 | 1.602 |

## 2.3 Input File Details

In this section, we detail the additional blocks and definitions required in BISON, which is a finite element-based nuclear fuel performance code, to leverage the ability to describe TRISO particle layer stiffness with spatial dependence, the computation of Mode $I$ SIF via the interaction integral, and the consideration of the gradient of the elasticity tensor along the crack propagation direction.

The functions "`elastic_mod_material`"and "`elastic_mod_material_der`" define the spatial evolution of the Young's modulus of the assumed isotropic materials comprising the SiC and the IPyC layers and its spatial derivative along the crack propagation direction, respectively. This spatial description of stiffness accounts for the stiffness of the SiC and PyC materials and an interface region on which the actual structural behavior is assumed to be a mix of both materials. We create materials with such spatially varying stiffness descriptions in the object "`generic_materials`" and we apply it to both the IPyC and SiC layers—which happen to be identified as blocks too. As discussed in Section 2.1, we require that both the elasticity tensor's spatial distribution and its gradient along the crack propagation direction, which are provided to the "`DomainIntegral`" input block via the "`functionally_graded_youngs_modulus`" and "`functionally_graded_youngs_modulus_crack_dir_gradient`" input parameters.

The extension of the methodology described in this chapter to cracks of orientations other than radial remains as future work.

## 2.4 Application to a TRISO Particle

The terms of the interaction integral developed in previous sections are used herein to assess the SIF of a Mode I crack through the IPyC layer. This metric can be used in assessing the possibility of crack propagation into the SiC layer. We set up a two-dimensional model of a TRISO particle, leveraging symmetry on both the X and Y planes and introducing a radial crack through the IPyC layer by omitting the Dirichlet boundary conditions where the fixed Y displacement boundary condition applied to all other layers is not applied to the IPyC layer (see Figure 2.4).

We use the similar material properties and inputs to the simulation as Jiang et al. (2022) (see baseline parameters with conditions "2" of Section 4.1 therein). Additionally, we assume that the interface between the SiC and iPyC layers is porous. From a mechanical standpoint, one consequence of such porosity is a smooth transition of the layer interface stiffness where the elasticity modulus does not vary sharply over the interface, but across a transition zone (see Arregui-Mena et al. (2021); Seibert et al. (2019) for a discussion on the experimental results). We employ a transition zone of $8\mu m$ to capture the material porosity on the iPyC-SiC interface. In our case, we use an elasticity modulus of 25 GPa for the iPyC layer, which transitions to a value of 312 GPa for the SiC layer outside the transition zone and that is functionally defined with a hyperbolic tangent of the type shown in Eq. 2.2. Note that the transition of a crack from a soft material to a stiffer material makes its failure probability less likely when a porous or transition zone exists (i.e., the layer interface can be described as a graded material and the failure can properly be modeled by the energy release of the J-integral).

Considering a transition zone of $8\mu m$, with the developed axisymmetric formulation and FGM

Listing 2.1. Input file excerpt for the addition of spatially-dependent Young's modulus and its use in the domain integral action.

```
[Functions]
  ...
  [elastic_mod_material_der]
    type = ParsedFunction
    symbol_names = 'Eipyc ESiC beta'
    symbol_values = '25e9 312e9 4e8'
    expression = '(ESiC-Eipyc) * x * beta * (1.0 - tanh(beta*(x*x+y*y-0.0003525*0.0003525)) * '
                 'tanh(beta*(x*x+y*y-0.0003525*0.0003525)))'
  []
  [elastic_mod_material]
    type = ParsedFunction
    symbol_names = 'Eipyc ESiC beta'
    symbol_values = '25e9 312e9 4e8'
    expression = '(Eipyc + ESiC) / 2 + (ESiC-Eipyc)/2 * tanh(beta*(x*x+y*y-0.0003525*0.0003525))'
  []
  ...
[]

[Materials]
  ...
  [generic_materials]
    type = GenericFunctionMaterial
    prop_names = 'elastic_mod_material_mat elastic_mod_material_der_mat'
    prop_values = 'elastic_mod_material elastic_mod_material_der'
  []
  ...
    [IPyC_SiC_elasticity_tensor]
    type = ComputeVariableIsotropicElasticityTensor
    youngs_modulus = elastic_mod_material_mat
    poissons_ratio = 0.21
    args = ''
    block = 'IPyC SiC'
  []
  ...
[]

[DomainIntegral]
  integrals = 'JIntegral InteractionIntegralKI'
  boundary = 9999
  radius_inner = '0.01e-3 0.005e-3 0.01e-3'
  radius_outer = '0.01e-3 0.005e-3 0.02e-3'
  crack_direction_method = CrackDirectionVector
  crack_direction_vector = '0 1 0'
  2d = true
  axis_2d = 2
  incremental = true
  symmetry_plane = 1

  functionally_graded_youngs_modulus = elastic_mod_material_mat
  functionally_graded_youngs_modulus_crack_dir_gradient = elastic_mod_material_der_mat

  temperature = temperature
  eigenstrain_names = 'SiC_thermal_eigenstrain IPyC_TE_strain'

  youngs_modulus = 169e9
  poissons_ratio = 0.21
  block = 'IPyC SiC'
[]
```

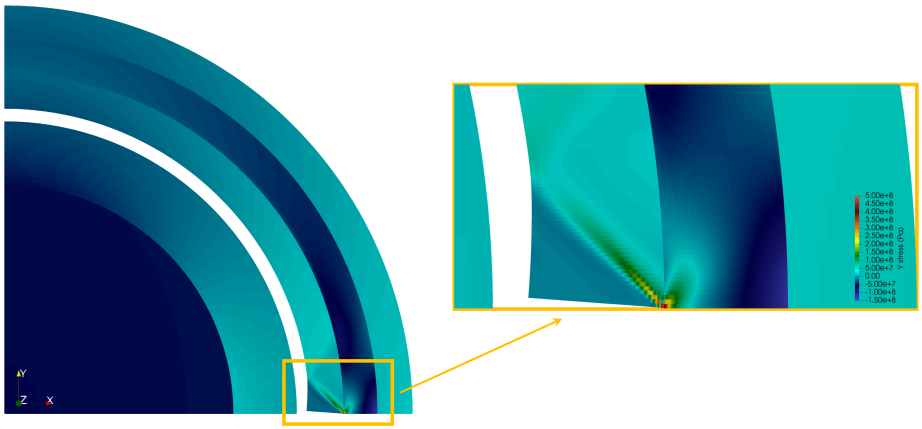

Figure 2.4. yy Cauchy stress component.

terms, the resulting SIF is $\approx 9.04\,\mathrm{MPa}\sqrt{\mathrm{m}}$. A comparison of SIFs with various lengths of the transition zone is shown in Table 2.3.

Table 2.3. Influence of porous zone length for the iPyC-SiC layer interface on the SIF characterizing the likelihood of propagation into the SiC layer.

| $4\mu m$ | $8\mu m$ | $12\mu m$ |
|---|---|---|
| $7.36\,\mathrm{MPa}\sqrt{\mathrm{m}}$ | $9.04\,\mathrm{MPa}\sqrt{\mathrm{m}}$ | $10.2\,\mathrm{MPa}\sqrt{\mathrm{m}}$ |

As expected, increasing the porosity layer thickness causes an increase in the resulting SIF (see Figure 2.3) since this type of crack grows from the relatively softer material into the stiffer material. Generic SiC materials can feature fracture toughness within the range of 4.0 to $9.0\,\mathrm{MPa}\sqrt{\mathrm{m}}$ (see Yuan et al. (2003)), depending on specific temperature conditions and material composition. For these reasons, an accurate description of the thermomechanics of the interface can be key to properly predicting the ability of the crack to propagate into the SiC layer.

# 3. SENSITIVITY STUDY

## 3.1 Mesh Sensitivity of the Fracture Mechanics Approach

As mentioned in Section 1, major limitations of the stress-based approach to fracture prediction combined with the Weibull distribution for determining failure probability include mesh dependency (see, e.g., Towse et al. (1999); Mitchell et al. (2003); Singh (2015)) and the consequent significant misestimation of the failure probability. When there is a stress concentration in the structure, either due to geometry or due to a developed discontinuity such as a crack, the stress computed at the quadrature points in the elements, located in the region of stress concentration, is greater than the experimental values. For the cases with a crack, the stress near the crack tip is greater due to a stress singularity condition (i.e., stress being infinite at the crack tip). The finer the mesh is, the higher the computed stress will be at the crack tip. Since the computed stress is mesh-dependent, the calculated failure probability using the stresses is also mesh-dependent, as shown in Figure 3.1. In addition, the stress term in the Weibull failure probability model ($\sigma/\sigma_0$) is raised to the power of the Weibull modulus (m), as shown in Equation 3.1. The high value of stress at or near the crack tip has shown to lead to overestimation of the failure probability in our results. The fracture mechanics-based approach overcomes this limitation.

$$P_f = 1 - \exp\left(-\int_V \left[\frac{\sigma}{\sigma_0}\right]^m \mathrm{d}V\right) \tag{3.1}$$

In the fracture mechanics approach, the SIF is used to estimate the stresses corrected near the crack tip. When the SIF increases and becomes equal to the fracture toughness of the material, the crack is assumed to propagate. The domain integral approach estimates the value of the SIF using the stress and strain in a domain that is located away from the crack tip. Since the stresses and strains used to compute the SIF are computed away from the crack tip, the obtained SIF is practically mesh independent, as shown in Figure 3.2. Use of domain integral approaches to the computation of SIF via the numerical integration of rings allows for avoiding singularity issues Yu and Kuna (2021). The failure probability obtained using a fracture mechanics approach is therefore not overestimated due to local stress concentration captured by finer meshes. The expression for the conditional probability of fracture initiation is given in equation 3.2. That approach, proposed already in Williams et al. (2016), has been applied to predict fracture in reactor pressure vessels using the same underlying Weibull model in Spencer et al. (2019). In that formula, $K_I$ can be obtained in a deterministic manner from the domain integral approach described in the first part

of this document.

$$P_f = 1 - \exp\left(-\left[\frac{K_I}{K_{Ic}}\right]^b\right) \tag{3.2}$$

where $K_I$ is the SIF, $K_{Ic}$ is the fracture toughness of the material, and $b$ is the Weibull modulus, an empirical parameter based on the distribution of the fracture toughness.

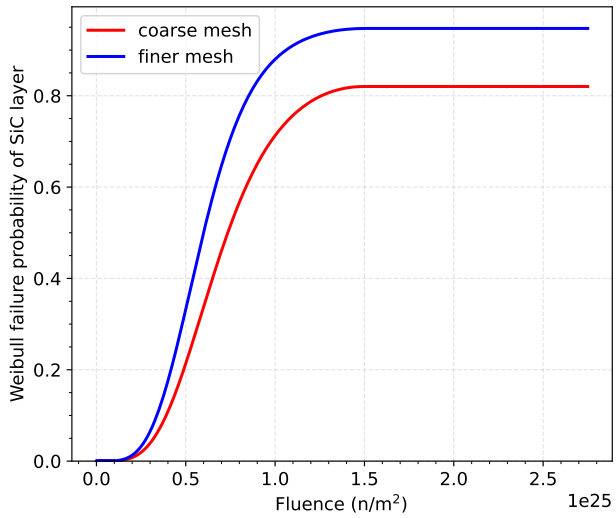


Figure 3.1. Dependence of the stress-based failure probability of SiC layer for two mesh densities. Coarse mesh has an element size of 1.54 $\mu$m, while finer mesh has a mesh size of 1.0 $\mu$m

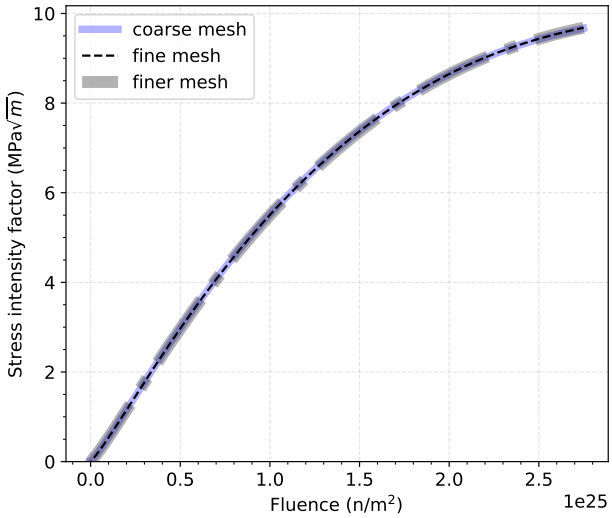


Figure 3.2. Dependence of the evaluated SIF with various levels of mesh refinement.

## 3.2 Sensitivity to Fracture Mechanics Approach Parameters

Figure 3.3 shows the schematic of the domain used for computing the SIF. The geometric parameters of the domain, inner radius, and width are also shown. Figures 3.4 and 3.5 show the influence of width and inner radius, respectively, on the computed SIF for a TRISO particle. The influence of the inner radius on the SIF seems to be stronger than that of the width[a]. Another assumption of this work refers to the evolution of the irradiation eigenstrain: (1) The SiC layer is assumed to not experience irradiation swelling; and (2) The radial gradient of the irradiation eigenstrain of the IPyC layer is considered to be significantly smaller than that of thermal eigenstrains for the purpose of computing the SIF with the interaction integral.

[a]Results shown here feature noticeable path dependency. This is likely due to the presence of creep (see Tiwari (2022) for a recent study on J-integral and C-integral as proxies for plastic and creep failure, respectively). Given this unresolved aspect of the present methodology, we would recommend shorter widths and an inner radius closer to the crack tips to obtain conservative estimates from the interaction integral.

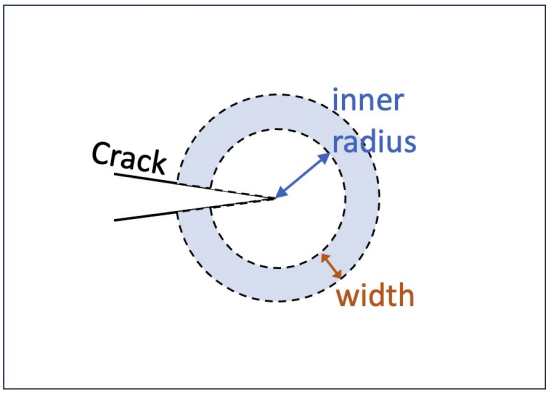


Figure 3.3. Inner radius and width of the domain used for evaluating the SIF.

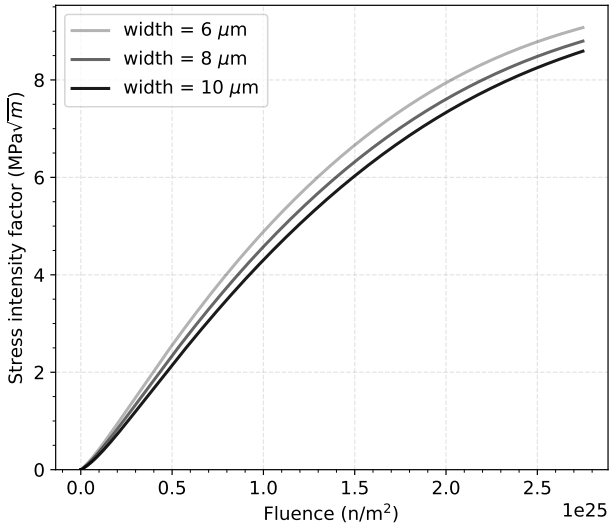


Figure 3.4. Sensitivity of SIF to the ring width.

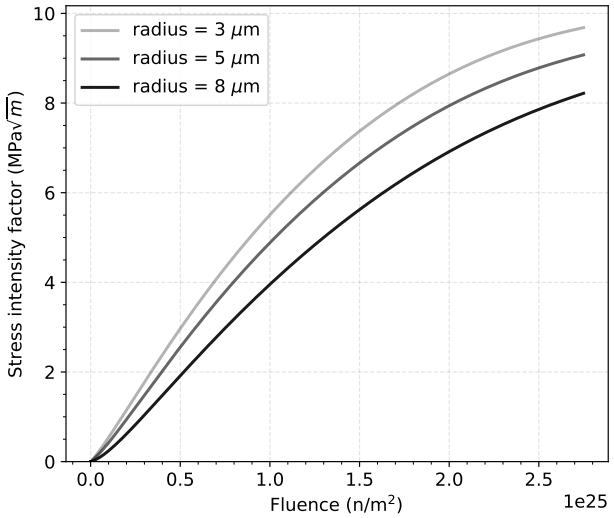


Figure 3.5. Sensitivity of SIF to the ring inner radius.

## 3.3 Sensitivity to TRISO Particle Parameters

The failure probability of the TRISO SiC layer assuming a crack in the IPyC layer is evaluated using the fracture mechanics-based approach. Equation 3.3 expresses the probability of failure of the SiC layer ($\mathrm{P}_{SiC_{failure}}$) in terms of the probability of failure of the IPyC layer ($\mathrm{P}_{PyC_{failure}}$), the probability of the IPyC layer remaining intact ($\mathrm{P}_{PyC_{intact}}$), the probability of failure of the SiC layer given that IPyC layer has failed ($\mathrm{P}_{SiC_{failure}|PyC_{failure}}$), and the probability of failure of the SiC layer given that the IPyC layer remains intact ($\mathrm{P}_{SiC_{failure}|PyC_{intact}}$):

$$P_{SiC_{failure}} = P_{PyC_{failure}} \times P_{SiC_{failure}|PyC_{failure}} + P_{PyC_{intact}} \times P_{SiC_{failure}|PyC_{intact}} \tag{3.3}$$

When the PyC layer is intact, the SiC layer stays in compression and the failure probability $\mathrm{P}_{SiC_{failure}|PyC_{intact}}$ is very small. In this section, the dependence of $\mathrm{P}_{SiC_{failure}|PyC_{failure}}$ and $\mathrm{P}_{PyC_{failure}} \cdot \mathrm{P}_{SiC_{failure}|PyC_{failure}}$ on several parameters is presented. (Note that the domain integral-based results always assume an existing IPyC crack.) The $K_{Ic}$ value is considered to be 3.46 MPa$\sqrt{m}$ and the $b$ parameter is considered to be 23 for the SiC layer for these analyses. These values for $K_{Ic}$ and $b$ are inferred from the normal distribution parameters for the fracture toughness of CVD $\beta$-SiC given in Snead et al. (2007). For the stress-based approach, the Weibull parameters for the SiC layer characteristic strength ($\sigma_o$) and Weibull modulus ($m$) are considered to be 9.64 MPa and 6.0, respectively (Miller et al. (2018)). Note that the fracture mechanics-based approach is used for evaluating $\mathrm{P}_{SiC_{failure}|PyC_{failure}}$, while $\mathrm{P}_{PyC_{failure}}$ is evaluated using stress-based approach.

The TRISO particle analyzed here has a spherical geometry, the fuel is UCO, and the irradiation temperature is 1573 K. The rest of the simulation conditions correspond to the parameters of Jiang et al. (2022) for the set of "conditions 3" (see Table 2 therein). Figures 3.6 and 3.7 show the sensitivity of $\mathrm{P}_{SiC_{failure}|PyC_{failure}}$ and $\mathrm{P}_{PyC_{failure}} \cdot \mathrm{P}_{SiC_{failure}|PyC_{failure}}$ to the ratio of elastic moduli

of SiC and PyC. To account for some sensitivity in the material's elastic moduli, we vary their ratio across the interface; thus, Figure 3.6 corresponds to the cases when the SiC elastic modulus is held constant and the PyC elastic modulus changes, while Figure 3.7 is for the cases when PyC elastic modulus is kept the same and the SiC elastic modulus varies. It can be noted from these figures that with an increase in the ratio of the elastic moduli of SiC and PyC, the failure probability decreases. The failure probability is smaller because the SIF is smaller. Intuitively, this means that a crack in a softer material will have increasing difficulty penetrating through the stiffer material as the relative stiffness (elastic modulus) of the stiffer material increases. After reaching a fluence of about 7.0 $\times 10^{24}$n/m$^2$, the $P_{SiC_{failure}|PyC_{failure}}$ reaches a value of 1.0, indicating that the SiC layer will fail at this point if the PyC layer is already cracked. The probability that both the PyC and SiC layers will fail ($P_{PyC_{failure}} \cdot P_{SiC_{failure}|PyC_{failure}}$) is also shown in Figure 3.6. Note that $P_{PyC_{failure}} \cdot P_{SiC_{failure}|PyC_{failure}}$ is much lower than $P_{SiC_{failure}|PyC_{failure}}$ because the failure probability of PyC layer is low. The figure indicates that the ratio of elastic moduli of SiC and PyC has a strong influence on the probability of failure of PyC and SiC.

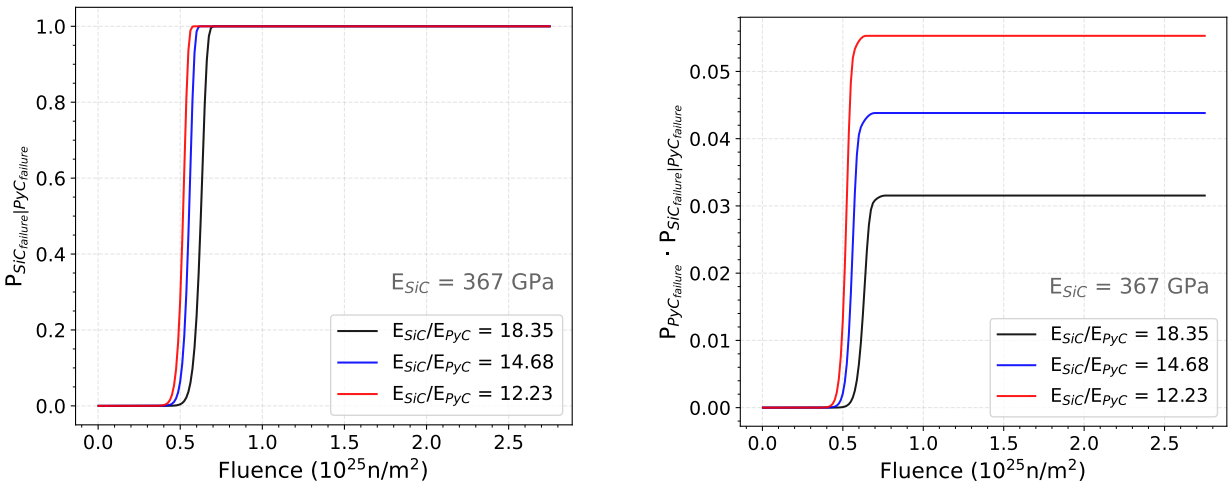


Figure 3.6. Sensitivity of fracture mechanics-based failure probability to the ratio of elasticity moduli of SiC and PyC layers, with the elastic modulus of the SiC layer held constant.

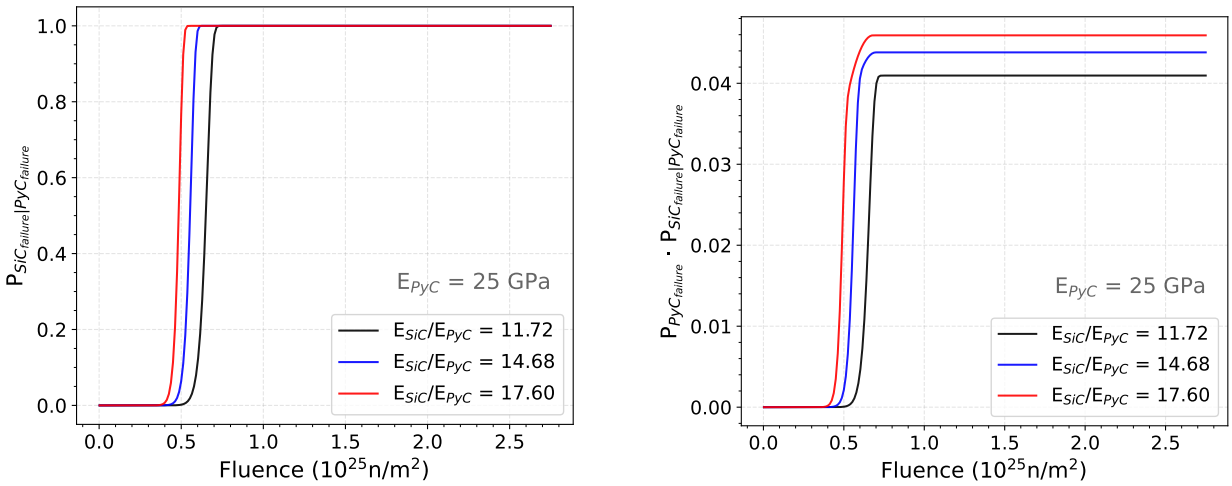


Figure 3.7. Sensitivity of fracture mechanics-based failure probability to the ratio of elasticity moduli of SiC and PyC layers, with the elastic modulus of the PyC layer held constant.

Figure 3.8 shows the dependence of the failure probabilities on the thickness of the SiC layer. The $P_{SiC_{failure}|PyC_{failure}}$ is found to be almost independent of the SiC layer thickness. The $P_{PyC_{failure}} \cdot P_{SiC_{failure}|PyC_{failure}}$ is found to be slightly dependent on the SiC layer thickness, which is due to the influence of the thickness on the $P_{PyC_{failure}}$.

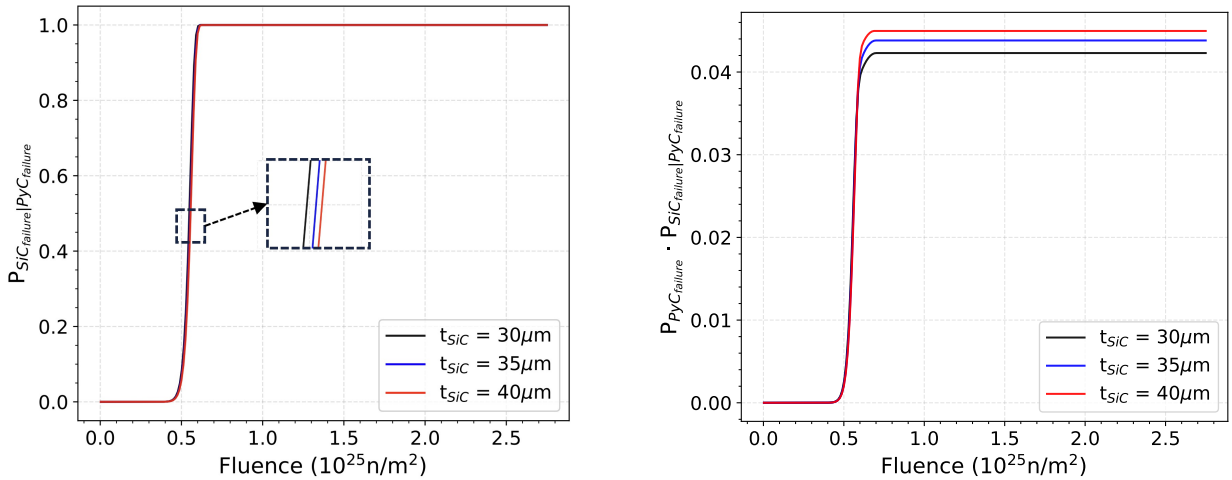


Figure 3.8. Sensitivity of fracture mechanics-based failure probability to the SiC layer thickness.

Figure 3.9 shows the influence of temperature on the failure probabilities obtained using the fracture mechanics approach. The primary effect of the temperature is on the creep behavior of the PyC layers. Due to greater creep at higher temperature, the stress exerted by the PyC layer on the

SiC layer (and vice-versa) is greatly reduced, leading to the reduced failure probability of the PyC and SiC layers. However, this phenomenon is true only when the PyC layer remains intact. When the IPyC layer has failed, the increased creep strain in the IPyC layer has hardly any influence on the failure of SiC, as can be noted from the $P_{SiC_{failure}|PyC_{failure}}$ versus fluence plot. Due to the reduced failure probability of the IPyC layer at elevated temperature, the failure probability $P_{PyC_{failure}} \cdot P_{SiC_{failure}|PyC_{failure}}$ is also significantly smaller at higher temperature.

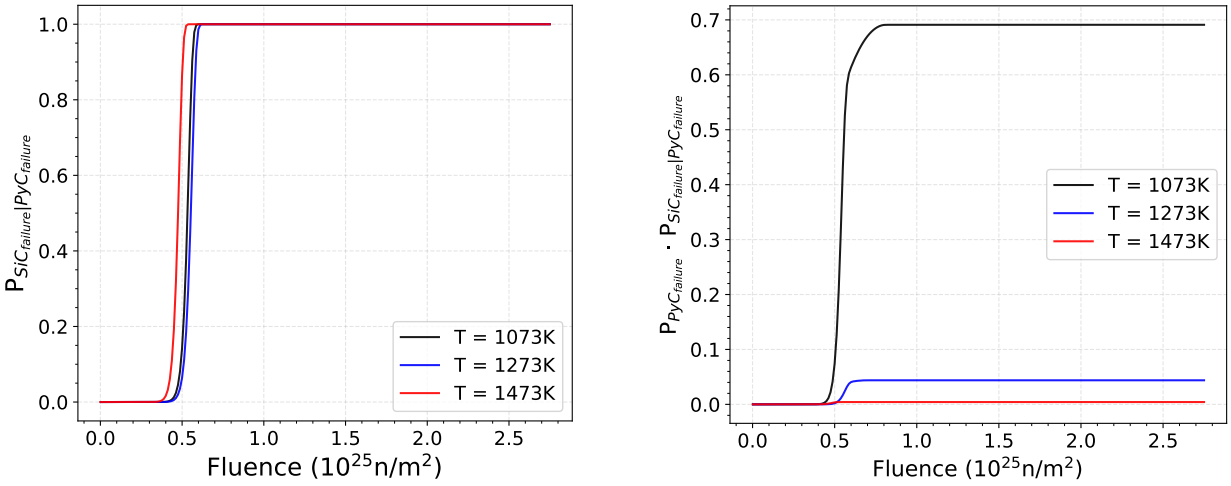


Figure 3.9. Dependence of fracture mechanics-based failure probability on the operating temperature.

As discussed in Section 2.4, we consider a transition region at the interface of the two material layers, IPyC and SiC, where the elastic properties of one layer gradually transitions to that of the other layer. The width of this transition region, which can be informed by laboratory experiments can be influenced by the manufacturing process and have an impact on the evaluated failure probability. Figure 3.10 shows the influence of the transition region thickness on the failure probabilities. It is clear from the figure that the transition region thickness has a strong influence on the failure probabilities. The thickness of the transition region can be obtained from the TRISO particle characterization; here we use values within the ranges reported in the literature (see Arregui-Mena et al. (2021)).

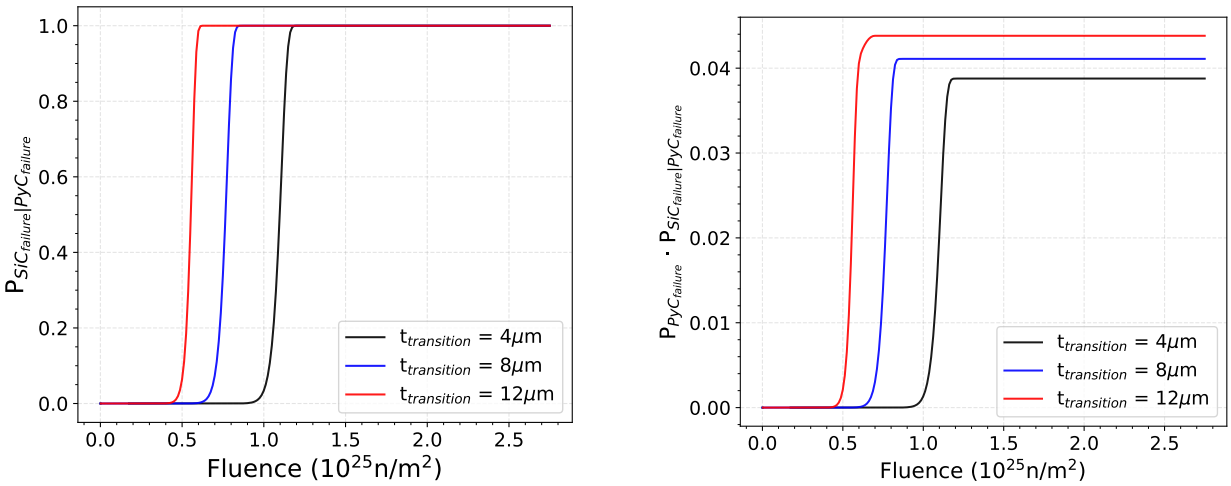


Figure 3.10. Dependence of fracture mechanics-based failure probability on the thickness of the IPyC-SiC transition zone.

## 3.4 Interaction Integral vs Stress-Based Failure Probability

Figure 3.11 and Figure 3.12 show a comparison of the failure probabilities obtained using the stress-based approach with the Weibull distribution and the fracture mechanics approach—note that the stress-based approach is mesh density sensitive; one mesh realization is chosen for comparison in this section. It can be noted from the figures that, during the initial fluence, the stress-based Weibull failure probability overestimates the failure probability and is much higher than the fracture mechanics-based failure probability. The rise in the fracture mechanics-based failure probability is much sharper than the one seen for the stress-based failure approach. Under the late-life fluence ($\geq$ 1.0 $\times 10^{25}$n/m$^2$), the difference in the failure probabilities from the two approaches becomes larger with an increase in temperature—at higher temperature the failure probabilities are lower and the relative difference between the probabilities from the two approaches is greater, while at lower temperatures the failure probabilities are higher and the relative difference is lower.

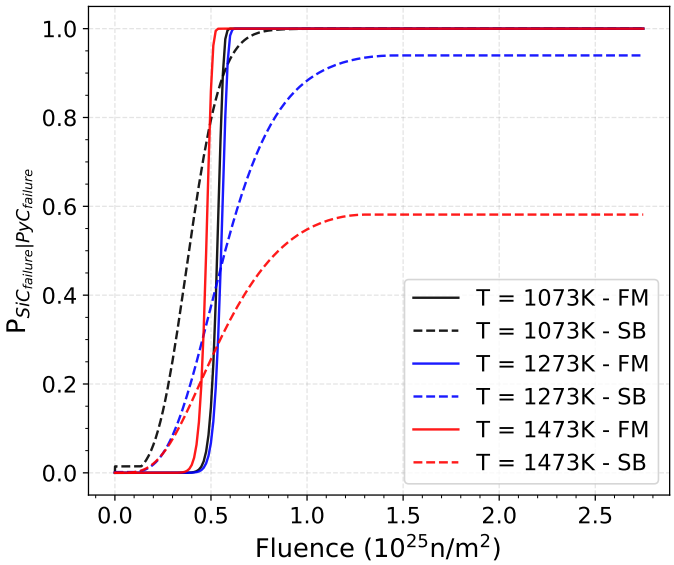


Figure 3.11. Comparison of stress-based (SB in the figure) and fracture mechanics (FM in the figure)-based SiC failure probability, given that the PyC layer has failed, at different temperatures.

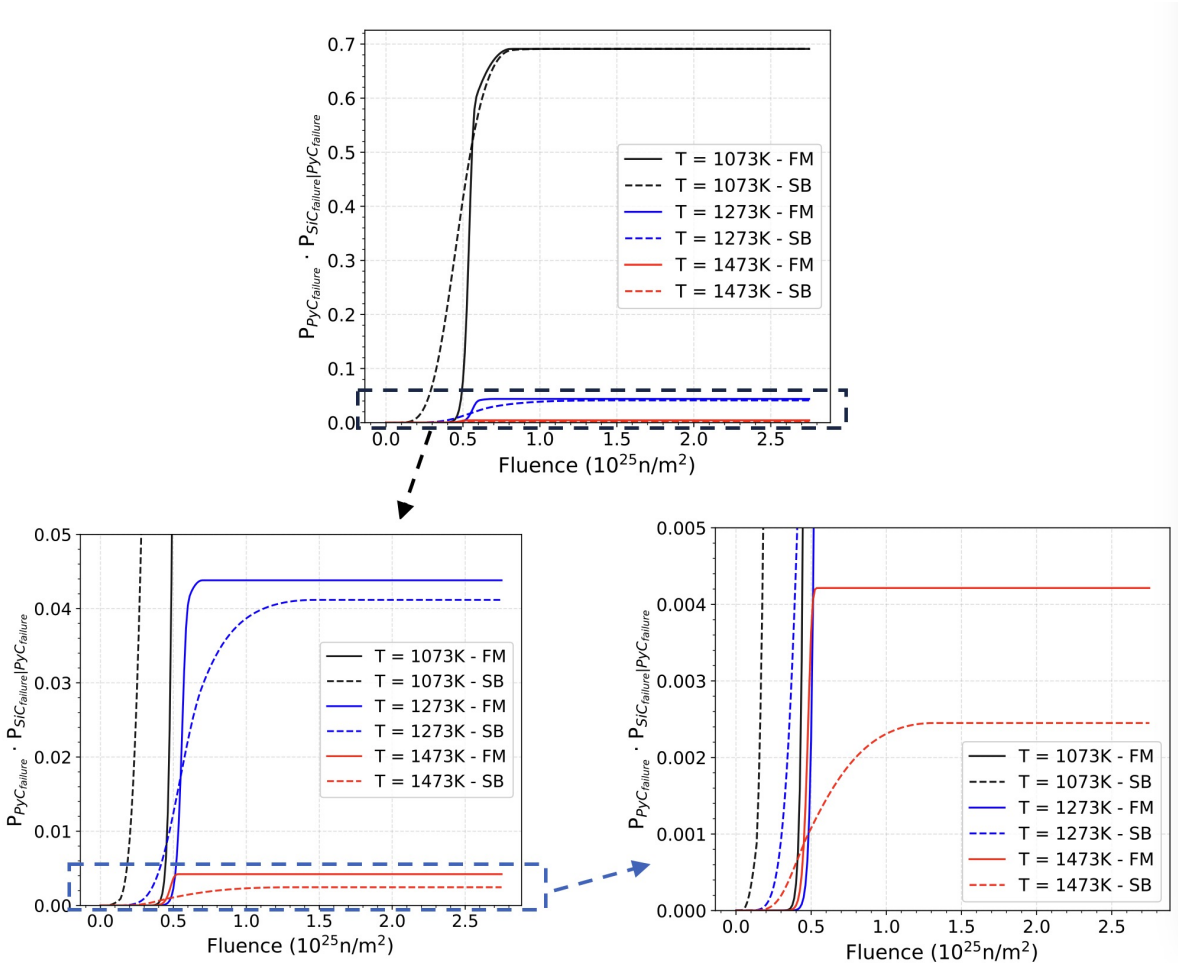


Figure 3.12. Comparison of stress-based (SB) and fracture mechanics (FM)-based failure probability of PyC and SiC layers at different temperatures.

## 3.5 Sensitivity to Fracture Toughness

In this section, we use the stress-based failure prediction approach to quantify the IPyC probability of failure (i.e. $P_{PyC_{failure}}$), whereas the failure of the SiC layer given a fully cracked IPyC layer (i.e. $P_{SiC_{failure}|PyC_{failure}}$) is computed with the interaction integral adapted to functionally-graded materials.

The conditional probability of failure (Equation 3.2) has two important material parameters: the fracture toughness ($K_{Ic}$) and its Weibull modulus $b$. These two parameters are material properties and are obtained empirically through mechanical testing. Figures 3.13 and 3.14 show the sensitivity of the failure probability with respect to the fracture toughness and its distribution, respectively. As the value of fracture toughness increases, the estimated failure probability decreases. As the value of distribution parameter increases, the failure probability rises. These results indicate that the failure probability is more sensitive to the fracture toughness value than its distribution parameter for reasonable values.

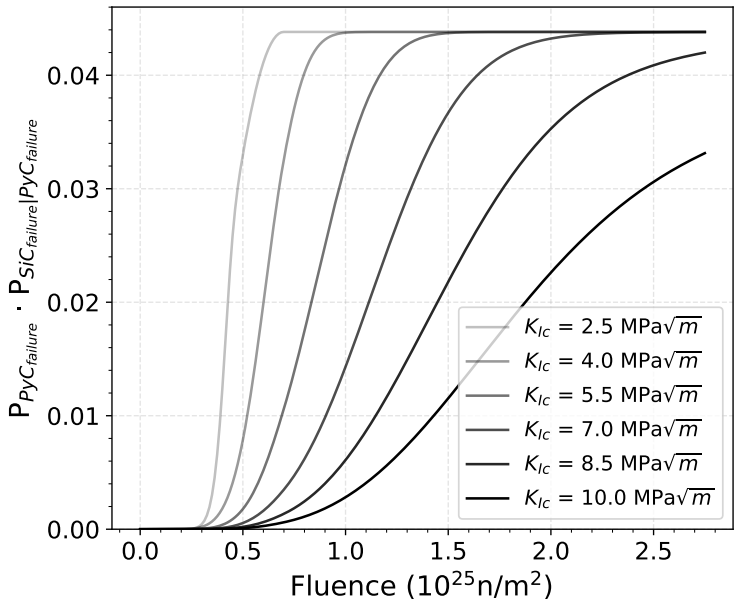


Figure 3.13. Sensitivity of the estimated failure probability to $K_{Ic}$ (b=10).

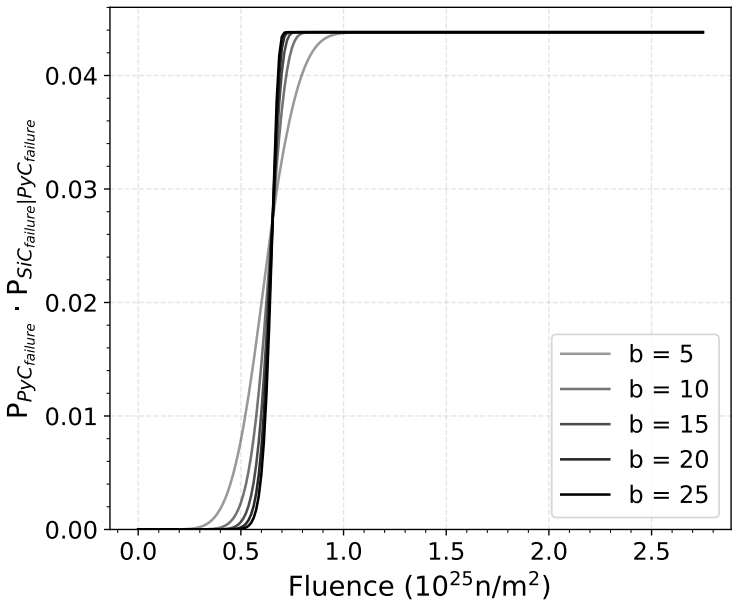


Figure 3.14. Sensitivity of estimated failure probability to the fracture toughness distribution distribution parameter b ($K_{Ic}$= 4.0 MPa$\sqrt{m}$).

## 3.6 Assessing Mesh-Distributed Tensile Strength on SiC Failure Behavior

As a separate exercise from previous sections and chapters—and in order to evaluate the stochastic failure of the SiC layer, a method for assessing a fracture based on distributed material properties was investigated. This method samples a normal distribution to determine the tensile strength at each quadrature point in the domain. As the tensile strength is exceeded, the elastic properties of the mesh are reduced to nearly zero. Releasing the SiC elastic strength after appropriate damage allows a pseudo-crack front to propagate through the material, thereby allowing the material to deform perpendicularly to the crack direction.

This method was investigated and tested briefly this year using simulated tensile specimens. In these simulations, a tensile bar was slowly loaded until a through-sample crack was detected.

As an initial approximation of the tensile strength, a normal distribution was used, which compares well with a 2-parameter Weibull distribution, to determine SiC material failure. An example of the tensile strength seeded across the mesh is shown in Figure 3.15. This distribution and its parameters are expected to change as more thorough model calibration and testing are performed. Because of the mesh-based sampling procedure, as mesh density is increased, the likelihood of low-strength elements acting as critical flaws increases. In order to adjust for this, a volume-weighting was applied to increase the material strength correspondingly. This allows similar Weibull failure criteria to be achieved for increasing mesh densities.

Figure 3.16 shows the progression of a crack front starting in the material using this fracture

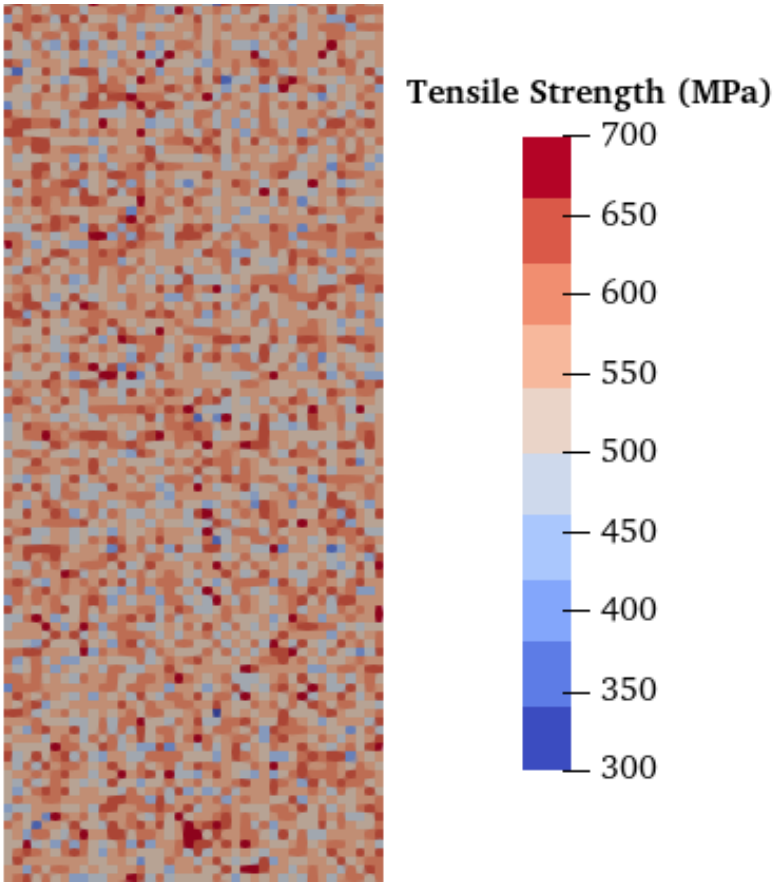


Figure 3.15. Example section of the mesh-based distribution of the SiC tensile strength across a tensile specimen.

method. Initially, elements near the sample periphery surpass the fracture strength and their elastic properties are reduced. This results in a local stress concentration where red colors are tensile stresses and blue are neutral, as shown in Figure 3.16.a. As the local stresses are increased due to the concentration, the crack slowly progresses across the material, further increasing the local stresses as more of the material is no longer load-bearing (see Figure 3.16.b). Finally, stresses across the sample increase beyond the fracture strength and the crack progresses across the material nearly instantly, resulting in a failed sample (see Figure 3.16.c).

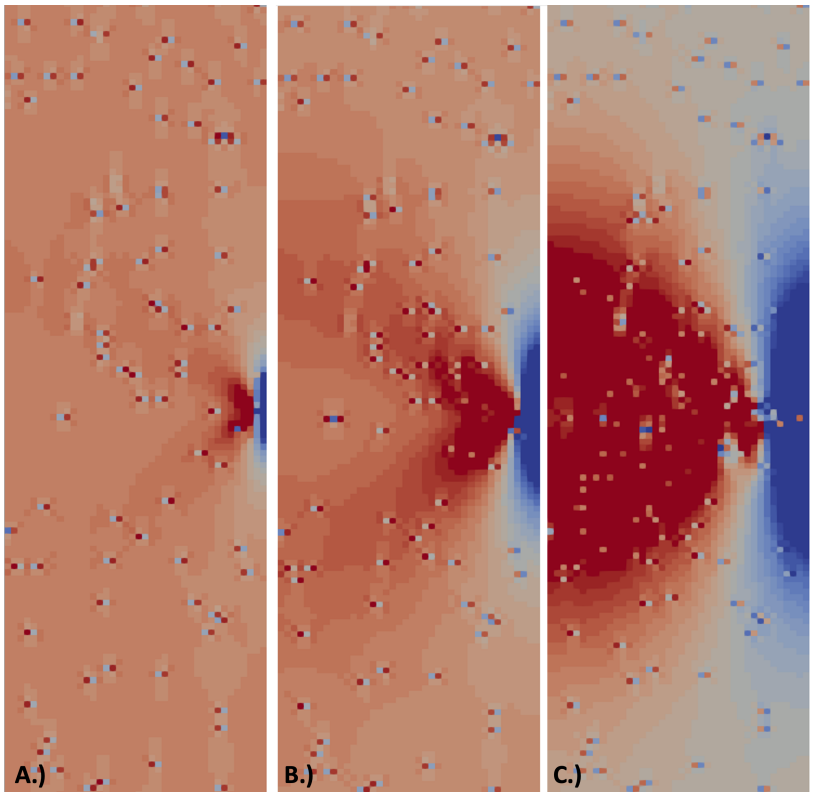


Figure 3.16. Illustration of the propagation of a crack front across a tensile specimen through the distribution of the axial stress.

This initial effort will allow future simulation of specific fracture experiments—specifically the hemispherical SiC crush tests that were used to derive the current fracture criteria. By duplicating the exact conditions the data was derived from, a more accurate fracture model can be developed and applied.

# 4. CONNECTION TO FISSION PRODUCT RELEASE

## 4.1 Fission Product Release Calculation using a Fracture Mechanics-based Approach

The use of fracture mechanics-based approaches to determine failure in TRISO coating layers have shown to yield higher fidelity models that can predict more accurately and consistently. As a coating layer is determined to be failed, it will lose its capability for fission product retention. In BISON, we utilize the Monte Carlo scheme to calculate the fission product release from all TRISO particles. Figure 4.1 depicts our methodology used to calculate the failure probability and fission product release of a population of TRISO particles using the fracture mechanics-based approach. Each analyzed particle is a realization of a set of statistically sampled parameters from the distributions of as-fabricated fuel characteristics (e.g., dimensions, densities, other parameters) that can be found among the particles in a fuel element. For each sample, BISON runs a one-dimensional/two-dimensional TRISO particle over the irradiation history. The standard stress-based Weibull approach will be used to evaluate the IPyC failure. When the IPyC is determined to be failed, the fracture mechanics approach will be used to compute the stress intensity factor $K_I$ and compare it with fracture toughness $K_{IC}$ of the SiC layer. If $K_I$ is greater than $K_{IC}$, then the SiC layer is failed and a large diffusivity (e.g., $10^{-6}$ $m^2/s$) will be assigned to model the loss of its retention power. After all the samples are finished, fission product release values from all TRISO particles will be summed together to provide the overall release amount. The impact of our new failure analysis approach on fission product release calculations will be demonstrated in the near future.

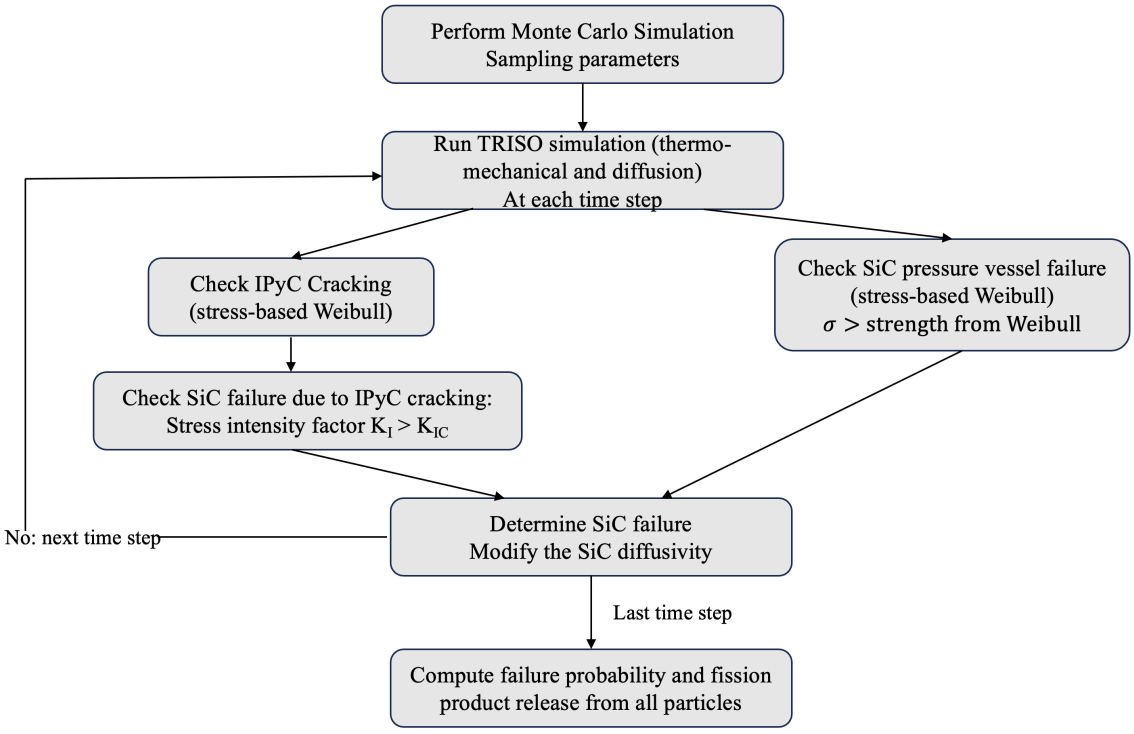


Figure 4.1. Methodology to predict failure probability and fission product release.

# 5. CONCLUSIONS AND FUTURE WORK

The stress-based approach to estimate failure probability has several shortcomings: over-estimation for structures having stress concentration, dependency on the finite element mesh-size, etc. For these reasons, such stress-based approach is not ideal for estimating the failure probability of structures having cracks. In the work presented herein, a fracture mechanics-based approach, involving computation of the interaction integral, to estimate the failure probability in functionally graded materials is presented. The demonstration examples on the TRISO fuel shows that the failure probability estimated using this approach is independent of the mesh and is likely to overestimation. A sensitivity study on the effect of parameters used for computing interaction integral, and the parameters for TRISO material properties (e.g., IPyC and SiC elastic moduli) and geometry (e.g., transition region width and SiC layer thickness) is performed to gain insights into the influence of these parameters on SIF and the estimated failure probability.

The current implementation of this approach, although it primarily considers the thermal strains, does not take other inelastic phenomena into account, such as creep and irradiation induced strains, into the failure probability prediction. The gradient of inelastic strains, if significant in magnitude, can affect the crack propagation and ultimately the failure probability of the structure. Future efforts should include incorporating these inelastic strains for computing the interaction integral value. The sensitivity study presented in this work does not extensively cover the thermo-mechanical properties of the TRISO particle layers, parameters of irradiation swelling model, and other geometric parameters. A deeper understanding of how the uncertainties in these properties and of the PyC and SiC layers translate to the uncertainties in the failure probability estimation is important.

A study on the application of volume-weighting to stress-based failure probability also remains as future work.

In this report, we have developed a fracture mechanics methodology for the analysis of fracture in TRISO particle layers; in particular, the structural failure of the SiC layer once the IPyC is already cracked. An analysis on the sensitivity of the fracture predictions with respect to the material properties (e.g., fracture toughness, interlayer porosity, model parameters) was also carried out. These analyses can allow the analysts to better quantify model uncertainties. The developed fracture modeling capability is intended to inform fission gas release calculations resulting from mechanical failure. Connecting the modeling of fracture mechanics and fission gas release will allow for better failure risk estimates. This critical multiphysics connection has not been addressed over the course of this fiscal year and is expected to be tackled in the near future.

# Bibliography


J. D. Arregui-Mena, R. L. Seibert, and T. J. Gerczak. Characterization of PyC/SiC interfaces with FIB-SEM tomography. *Journal of Nuclear Materials*, 545:152736, 2021.

W. Jiang, G. Singh, J. D. Hales, A. Toptan, B. W. Spencer, S. R. Novascone, S. L. N. Dhulipala, and Z. M. Prince. Efficient high-fidelity TRISO statistical failure analysis using bison: Applications to AGR-2 irradiation testing. *J. Nucl. Mater.*, 562:153585, 2022. doi:10.1016/j.jnucmat.2022.153585.

J.-H. Kim and G. H. Paulino. An accurate scheme for mixed-mode fracture analysis of functionally graded materials using the interaction integral and micromechanics models. *International Journal for Numerical Methods in Engineering*, 58(10):1457–1497, 2003.

J.-H. Kim and G. H. Paulino. Consistent formulations of the interaction integral method for fracture of functionally graded materials. *Journal of Applied Mechanics*, 72(3):351–364, 07 2004.

G.K. Miller, D.A. Petti, J.T. Maki, D.L. Knudson, , and W.F. Skerjanc. PARFUME Theory and Model Basis Report. Report INL/EXT-08-14497 (Rev.1), Idaho National Laboratory, September 2018.

B. C. Mitchell, J. Smart, S. L. Fok, and B. J. Marsden. The mechanical testing of nuclear graphite. *Journal of Nuclear Materials*, 322(2-3):126–137, 2003.

R. Nahta and B. Moran. Domain integrals for axisymmetric interface crack problems. *International Journal of Solids and Structures*, 30(15):2027–2040, 1993.

B. N. Rao and S. Rahman. Mesh-free analysis of cracks in isotropic functionally graded materials. *Engineering Fracture Mechanics*, 70(1):1–27, 2003. doi:10.1016/S0013-7944(02)00038-3.

R. L. Seibert, B. C. Jolly, M. Balooch, D. P. Schappel, and K. A.å Terrani. Production and characterization of TRISO fuel particles with multilayered SiC. *Journal of Nuclear Materials*, 515:215–226, 2019.

M. Shariati, M. M. Rokhi, and H. Rayegan. Investigation of stress intensity factor for internal cracks in fg cylinders under static and dynamic loading. *Frattura ed Integrità Strutturale*, 11(39): 166–180, 2017.

Gyanender Singh. *Explicit Crack Modeling based Approach for Structural Integrity Assessment of Brittle and Quasi-Brittle Structures*. PhD thesis, University of Minnesota, 2015.

L. L. Snead, T. Nozawa, Y. Katoh, T.-S. Byun, S. Kondo, and D. A. Petti. Handbook of SiC properties for fuel performance modeling. *Journal of Nuclear Materials*, 371(1):329–377, 2007. doi:10.1016/j.jnucmat.2007.05.016. Nuclear Fuels and Structural Materials 1.

B. W. Spencer, W. M. Hoffman, and M. A. Backman. Modular system for probabilistic fracture mechanics analysis of embrittled reactor pressure vessels in the Grizzly code. *Nuclear Engineering and Design*, 341:25–37, 2019.

A. Tiwari. Effect of material inhomogeneity under creep and plastic to creep transition of cracks. *Procedia Structural Integrity*, 39:290–300, 2022.

A. Towse, K. D. Potter, M. R. Wisnom, and R. D. Adams. The sensitivity of a weibull failure criterion to singularity strength and local geometry variations. *International journal of adhesion and adhesives*, 19(1):71–82, 1999.

T. Van-Xuan and G. Samuel. Development and industrial applications of X-FEM axisymmetric model for fracture mechanics. *Engineering Fracture Mechanics*, 82:135–157, 2012. doi:10.1016/j.engfracmech.2011.12.002.

T. C. Wang and P. Ståhle. Stress state in front of a crack perpendicular to bimaterial interface. *Engineering Fracture Mechanics*, 59(4):471–485, 1998. doi:10.1016/S0013-7944(97)00150-1.

P.T. Williams, T.L. Dickson, B. R. Bass, and H. B. Klasky. Fracture Analysis of Vessels – Oak Ridge, FAVOR, v16.1, computer code: Theory and implementation of algorithms, methods, and correlations. Technical Report ORNL/LTR-2016/309, Oak Ridge National Laboratory, Oak Ridge, TN, September 2016. URL `https://www.nrc.gov/docs/ML1627/ML16273A033.pdf`.

H. Yu and M. Kuna. Interaction integral method for computation of crack parameters K–T–A review. *Engineering Fracture Mechanics*, 249:107722, 2021.

R. Yuan, J. J. Kruzic, X. F. Zhang, L. C. De Jonghe, and R. Ritchie. Ambient to high-temperature fracture toughness and cyclic fatigue behavior in al-containing silicon carbide ceramics. *Acta Materialia*, 51(20):6477–6491, 2003.